CM² MAGAZINE

第 102 期

南方科技大学海洋磁学中心主编

http://cm2.sustech.edu.cn/

创刊词

海洋是生命的摇篮，是文明的纽带。地球上最早的生命诞生于海洋，海洋里的生命最终进化成了人类，人类的文化融合又通过海洋得以实现。人因海而兴。

人类对海洋的探索从未停止。从远古时代美丽的神话传说，到麦哲伦的全球航行，再到现代对大洋的科学钻探计划，海洋逐渐从人类敬畏崇拜幻想的精神寄托演变成可以开发利用与科学研究的客观存在。其中，上个世纪与太空探索同步发展的大洋科学钻探计划将人类对海洋的认知推向了崭新的纬度：深海（deep sea）与深时（deep time）。大洋钻探计划让人类知道，奔流不息的大海之下，埋藏的却是亿万年的地球历史。它们记录了地球板块的运动，从而使板块构造学说得到证实；它们记录了地球环境的演变，从而让古海洋学方兴未艾。

在探索海洋的悠久历史中，从大航海时代的导航，到大洋钻探计划中不可或缺的磁性地层学，磁学发挥了不可替代的作用。这不是偶然，因为从微观到宏观，磁性是最基本的物理属性之一，可以说，万物皆有磁性。基于课题组的学科背景和对海洋的理解，我们对海洋的探索以磁学为主要手段，海洋磁学中心因此而生。

海洋磁学中心，简称 CM^2，一为其全名“Centre for Marine Magnetism”的缩写，另者恰与爱因斯坦著名的质能方程 $E = MC^2$ 对称，借以表达我们对科学巨匠的敬仰和对科学的不懈追求。

然而科学从来不是单打独斗的产物。我们以磁学为研究海洋的主攻利器，但绝不仅限于磁学。凡与磁学相关的领域均是我们关注的重点。为了跟踪反映国内外地球科学特别是与磁学有关的地球科学领域的最新研究进展，海洋磁学中心特地主办 CM^2 Magazine，以期与各位地球科学工作者相互交流学习、合作共进！

“海洋孕育了生命，联通了世界，促进了发展”。21 世纪是海洋科学的时代，由陆向海，让我们携手迈进中国海洋科学的黄金时代。

目录

1. 欧洲鸣禽根据地磁信号停止迁徙达到繁殖地

翻译人：柳加波 liujb@sustech.edu.cn

Wynn J, Padget O, Mouritsen H, et al. ***Magnetic stop signs signal a European songbird's arrival at the breeding site after migration[J]****. Science, 2022, 375(6579): 446-449.*

https://doi.org/10.1126/science.abj4210

摘要：众所周知，鸟类可以非常精确地返回它们的繁殖地，但它们如何知道何时何地停止迁徙仍然是个谜。本文利用欧亚芦苇莺（Acrocephalus scirpaceus）近一个世纪以来的环志数据，讨论地球磁场的波动是否可以预测鸟类返回地点的变化。环志数据表明，鸟类在出发前记忆了磁倾角，之后在重新定位出生地或繁殖地时作为单坐标“停止标志”。虽然许多位置具有相同的倾角，来自不同迁徙方向的种群数据表明，在继承的返回航线上，鸟类会在第一个匹配正确倾角的地方停下来，从而解决这种不确定性。

ABSTRACT: Although it is known that birds can return to their breeding grounds with exceptional precision, it has remained a mystery how they know when and where to stop migrating. Using nearly a century's worth of Eurasian reed warbler (Acrocephalus scirpaceus) ringing recoveries, we investigated whether fluctuations in Earth's magnetic field predict variation in the sites to which birds return. Ringing recoveries suggest that magnetic inclination is learned before departure and is subsequently used as a uni-coordinate "stop sign" when relocating the natal or breeding site. However, many locations have the same inclination angle. Data from populations with different migratory directions indicate that birds solve this ambiguity by stopping at the first place where the right inclination is encountered on an inherited return vector.

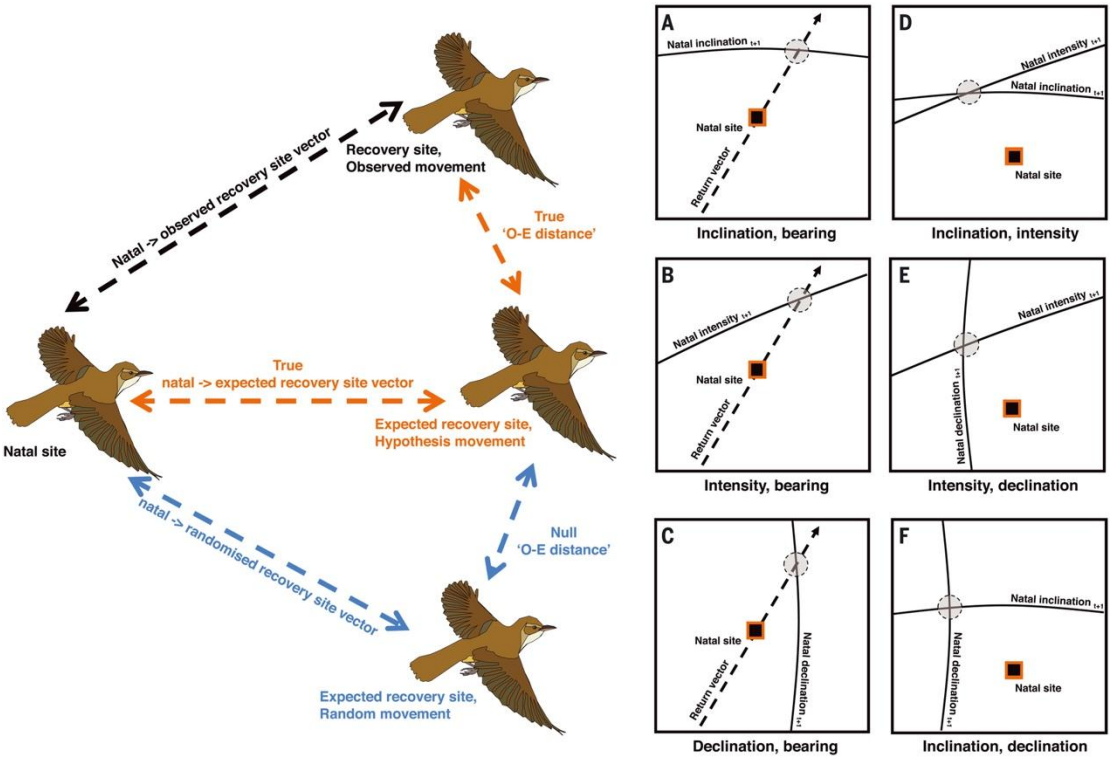

Figure 1. Using the observed-versus-expected distance to test navigational hypotheses.(Left) The observed-versus-expected distance between the hypothesized and observed recovery sites (true O-E distance) can be calculated and compared with the distance between the hypothesized recovery site and the recovery site expected under equal but random movements (null O-E distance). Through this comparison, we can calculate the likelihood of a hypothesis outperforming chance. (A to F) Diagrams showing how expected recovery positions under each hypothesis are calculated.

2. 渐新世—中新世分界甲烷水合物的分解

翻译人：张亚南 zhangyn3@mail.sustech.edu.cn

Kim B, and Zhang Y G. ***Methane hydrate dissociation across the Oligocene-Miocene boundary*** *[J]. Nature Geoscience, 2022.*

https://doi.org/10.1038/s41561-022-00895-5

摘要: 长期以来，甲烷水合物分解一直被认为是地球历史上造成全球碳循环扰动、气候变化，甚至大规模生物灭绝的原因。然而，与这些事件相一致的水合物不稳定和甲烷释放直接证据却少之又少。文中，作者展示了南大洋 3 个站位的脂质生物标志物的存在和碳同位素负漂，其直接与渐新世—中新世分界（23 Ma）的甲烷释放及随之而来的氧化状态相关。生物标志物证据表明，水合物的不稳定始于渐新世—中新世分界的最大冰期和低海平面时期，与模型结果一致。表明了静水压力的降低削弱了全球水合物稳定带的稳定性。海水中甲烷的氧化消耗水体中的氧气并造成酸化，这可能是促进中新世早期冰期快速终止的一种负反馈过程。

ABSTRACT: Methane hydrate dissociation has long been considered as a mechanism for global carbon cycle perturbations, climate change and even mass extinctions in Earth's history. However, direct evidence of hydrate destabilization and methane release coinciding with such events is scarce. Here we report the presence of diagnostic lipid biomarkers with depleted carbon isotopes from three sites in the Southern Ocean that are directly linked to methane release and subsequent oxidation across the Oligocene–Miocene boundary (23 million years ago). The biomarker evidence indicates that the hydrate destabilization was initiated during the peak of the Oligocene–Miocene boundary glaciation and sea-level low stand, consistent with our model results suggesting the decrease in hydrostatic pressure eroded the base of global methane hydrate stability zones. Aerobic oxidation of methane in seawater consumes oxygen and acidifies the ocean, acting as a negative feedback that perhaps facilitated the rapid and mysterious termination of glaciation in the early Miocene.

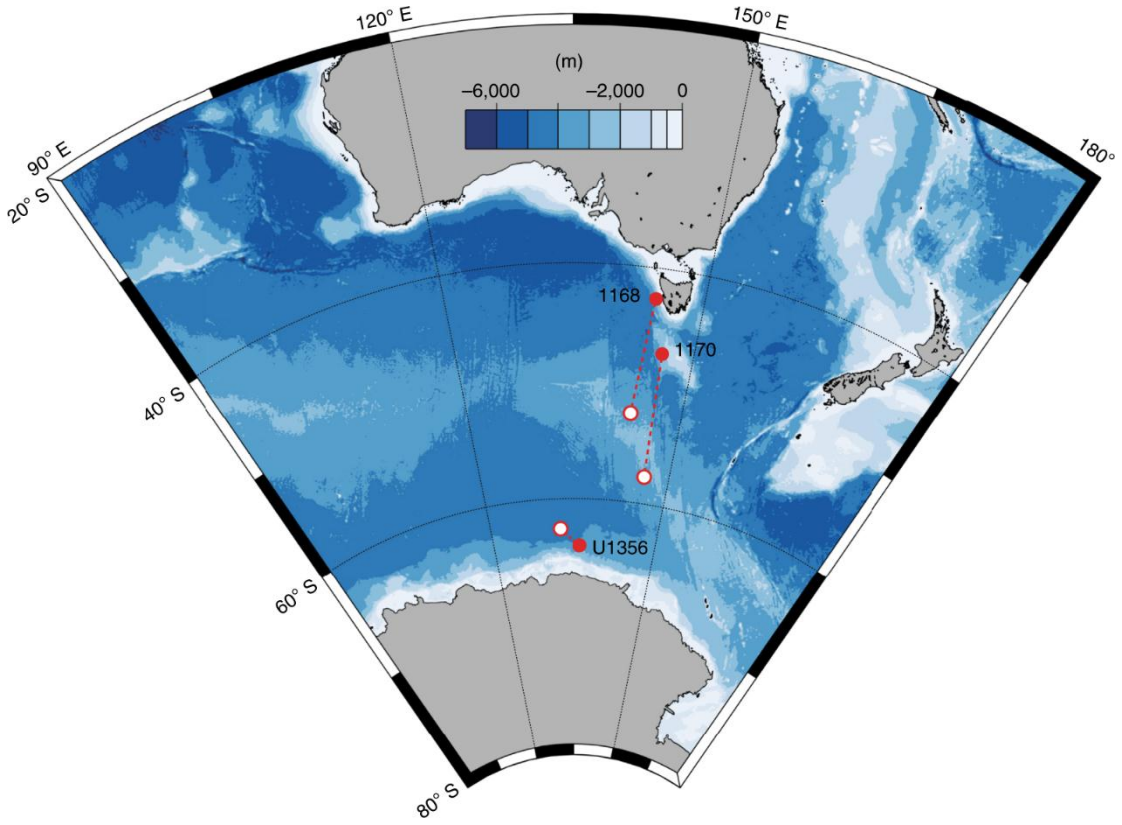

Figure 1. Location of our studied sites. ODP sites 1168 and 1170 and IODP site U1356 are overlaid on a map of modern-day bathymetry from the 2-min Gridded Global Relief Data (ETOPO246). Red filled circles indicate modern locations and white circles outlined in red indicate reconstructed palaeo-locations at 23 Ma using the GPlates software (Methods). Note that the red dashed lines do not indicate the actual migration of each site.

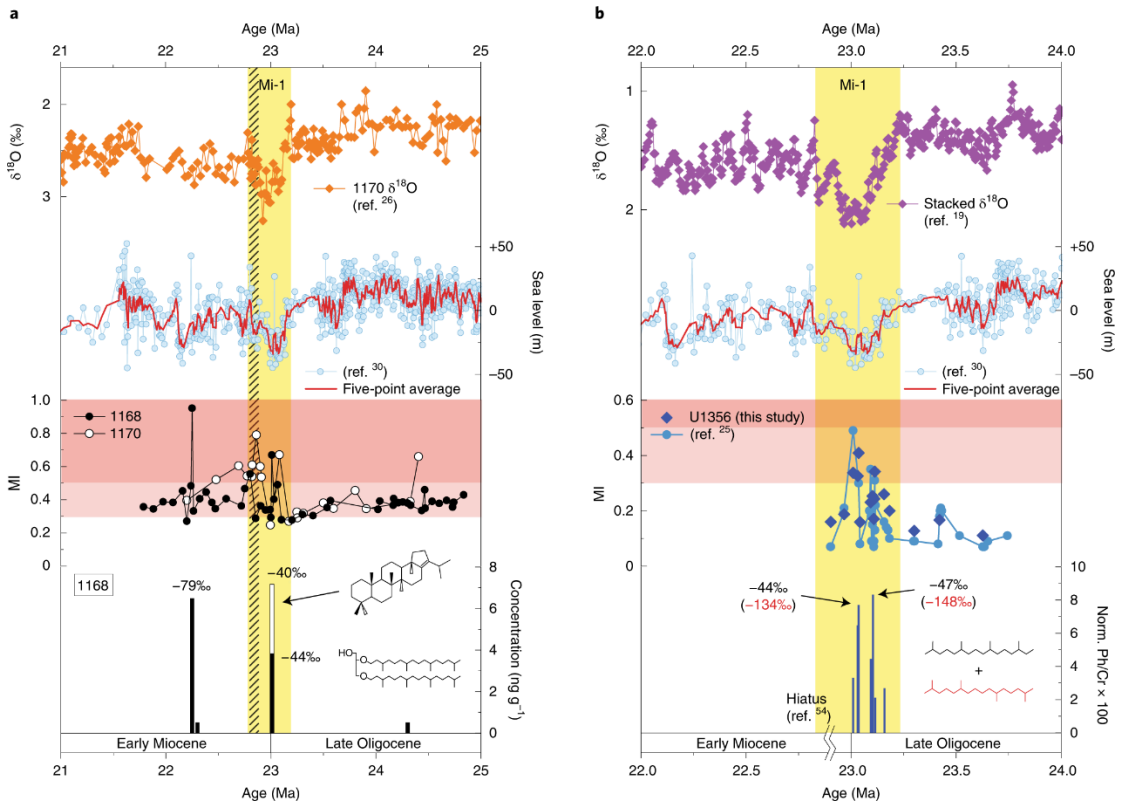

Figure 2. Coupling between late Oligocene–early Miocene global climate/sea-level and gas hydrate dissociation in the Southern Ocean. a, Plots of oxygen isotope ($\delta^{18}O$, orange) of benthic foraminifera at site 1170, eustatic sea-level reconstruction (light blue) and five-point average (red line), MI values of sites 1168 (black) and 1170 (white), concentrations of hop-17(21)-ene (white bar; structure shown) and archaeol (black bar; structure shown) and their compound-specific carbon isotopic ($\delta^{13}C$) signatures at site 1168. Compounds that are under the detection limit are not shown here (Extended Data Table 2). b, Stacked $\delta^{18}O$ of benthic foraminifera (purple), eustatic sea-level reconstruction (light blue) and five-point average (red line), MI values of site U1356 (this study and ref. 25), normalized phytane/crocetane (structures shown in black and red, respectively) concentration and its compound-specific $\delta^{13}C$ values. δ13C values in red indicate the calculated $\delta^{13}C$ value of crocetane (Methods). Yellow shaded areas highlight the Mi-1 event, and the hashed vertical line indicates the carbonate dissolution event41. A hiatus is situated after the Mi-1 event, punctuating the early Miocene records of site U1356 (Methods).

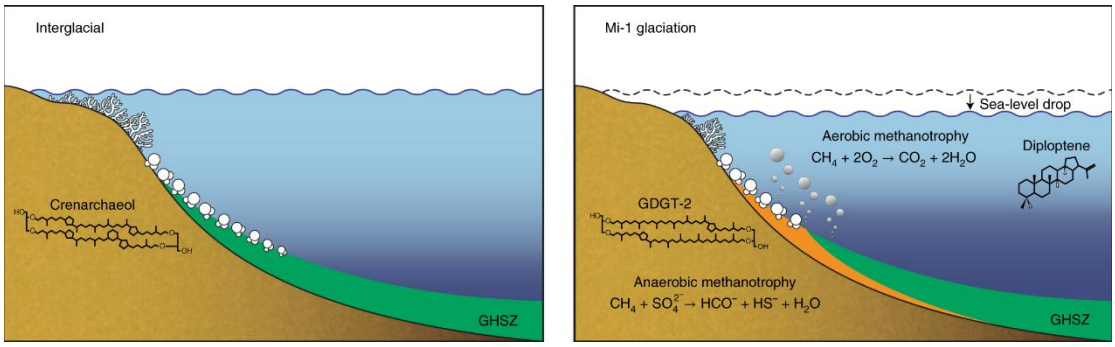

Figure 3. Schematic of changes of the GHSZ during interglacial and Mi-1 (peak glacial) conditions. The loss of GHSZ (GHSZ shown in green) in marine sediments (orange) is due to the drop in sea level during glaciation. Archaea associated with AOM preferentially synthesize GDGT-1, -2 (structure shown in the 'Mi-1 glaciation' panel) and -3 relative to crenarchaeol (structure shown in the 'Interglacial' panel), which typically dominates in normal marine sediments. Aerobic methane oxidation by bacteria produces diagnostic hopanoids such as diploptene, which could also be preserved in sediments. During the peak glaciation and afterwards, a release of hydrate-derived methane (grey bubbles) would result in anaerobic and aerobic methane oxidation, with the latter contributing to ocean acidification and potentially responsible for the seafloor carbonate dissolution event during the deglaciation.

3. 上新世以来日本海氧化还原历史的构造和轨道周期印迹

翻译人：刘伟 inewway@163.com

Zhao D, Wan S, Zhai L, et al. ***Tectonic and orbital imprints in the redox history of Japan Sea since the Pliocene*** *[J]. Paleoceanography and Paleoclimatology, 2022.*

https://doi.org/ 10.1029/2021PA004333.

摘要：深海氧含量在生物地球化学过程中起着至关重要的作用，对全球碳循环有着重要的影响。日本海是一个半封闭盆地，其与西北太平洋有浅水连接，其氧化还原历史受构造活动和气候变化的影响。对上新世以来日本海古氧化还原状态变化的研究主要集中在构造尺度上，轨道尺度上的研究至今尚缺乏。本文研究了日本海 IODP U1425 孔和 U1430 孔 4 Ma 以来的的高分辨率古氧化还原记录。自生 U 和 U/Al 记录表明，在 1.7 Ma 时，日本海氧化还原过程发生了明显的变化，从相对氧化状态转变为周期性的氧化-缺氧状态。这主要是由于上新世晚期至更新世早期日本东北部抬升导致北太平洋富氧水输入受限，以及 1.7 Ma 以来冰期-间冰期旋回海平面变化导致对马海峡打开和对马暖流周期性侵入所致。日本海氧化还原历史的轨道变化暗示了近 4 Ma 东亚夏季风降水演化的 400 ka 长偏心率周期的存在。海平面升降的振幅变化和对马暖流的流入以及东亚季风的演化，造成了日本海上 1.7 Ma 后氧化还原状态的偏心率和倾角周期，以及中更新世气候转型期前后的冰期从相对氧化状态转变到缺氧状态。

ABSTRACT: Oxygen content in deep ocean plays a vital role in biogeochemical processes and has significant impacts on global carbon cycle. The Japan Sea is a semi-closed basin with only shallow water connection to the Western North Pacific, and its redox history has been sensitively affected by tectonic and climatic changes in the past. Studies of paleo-redox changes in the Japan Sea focused on the tectonic and orbital scales since the Pliocene remain scarce to date. Here we present two high-resolution paleo-redox records during the last 4 Ma at IODP Sites U1425 and U1430 drilled in the Japan Sea. Our authigenic U (uranium) and U/Al records suggest remarkable changes of Japan Sea redox history from relatively oxic to periodic oxic-anoxic conditions at ~1.7

Ma. This was mainly caused by the restricted input of North Pacific oxygen-rich water due to the uplift of northeastern Japan during late Pliocene and early Pleistocene, and opening of Tsushima Strait and periodic intrusion of Tsushima Warm Current following sea-level change during glacial-interglacial cycles since ~1.7 Ma. Orbital changes of Japan Sea redox history suggest the existence of long eccentricity cycle of 400-ka associated with East Asian summer monsoon rainfall evolution throughout the last 4 Ma. Changes of the amplitude of sea-level and inflow of Tsushima Warm Current combined with the East Asian monsoon evolution produced eccentricity and obliquity cycles in Japan Sea redox environment after ~1.7 Ma, as well as a transition from relatively oxic to anoxic condition during glacials before and after Middle Pleistocene Transition.

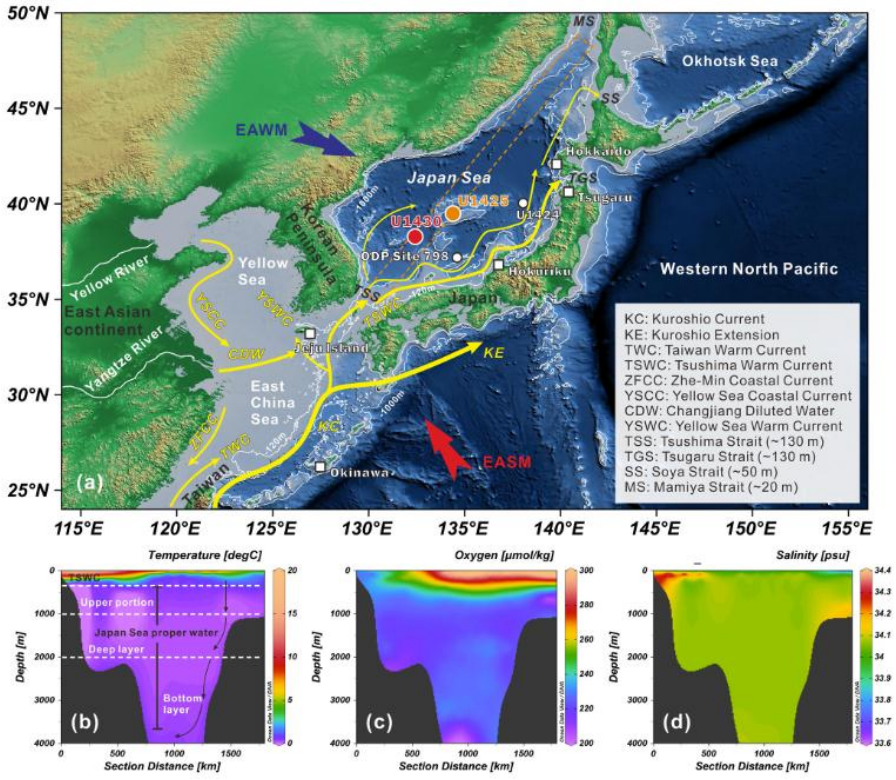

Figure 1. (a) Map showing the location of the IODP Site U1425 and U1430, bathymetry of the Japan Sea, and the flow of surface currents (yellow arrow lines). The referenced ocean sites and on-land geological sections are shown with white dots and squares, respectively. EAWM and EASM are shown with deep blue and red arrows, respectively. The orange dashed area from the southwest to the northeast of the Japan Sea indicates the selected section to show the water physicochemical property of this region. (b) Water temperature along the cross section shown in the orange dashed area in (a). The black arrow lines indicate the water mass sinking of the cooled TSWC. (c–d) The

same as (b) but for oxygen content and salinity. Data of the temperature, oxygen, and salinity are from World Ocean Atlas 2018. Sections of (b–d) were generated with Ocean Data View software (http://odv.awi.de/)

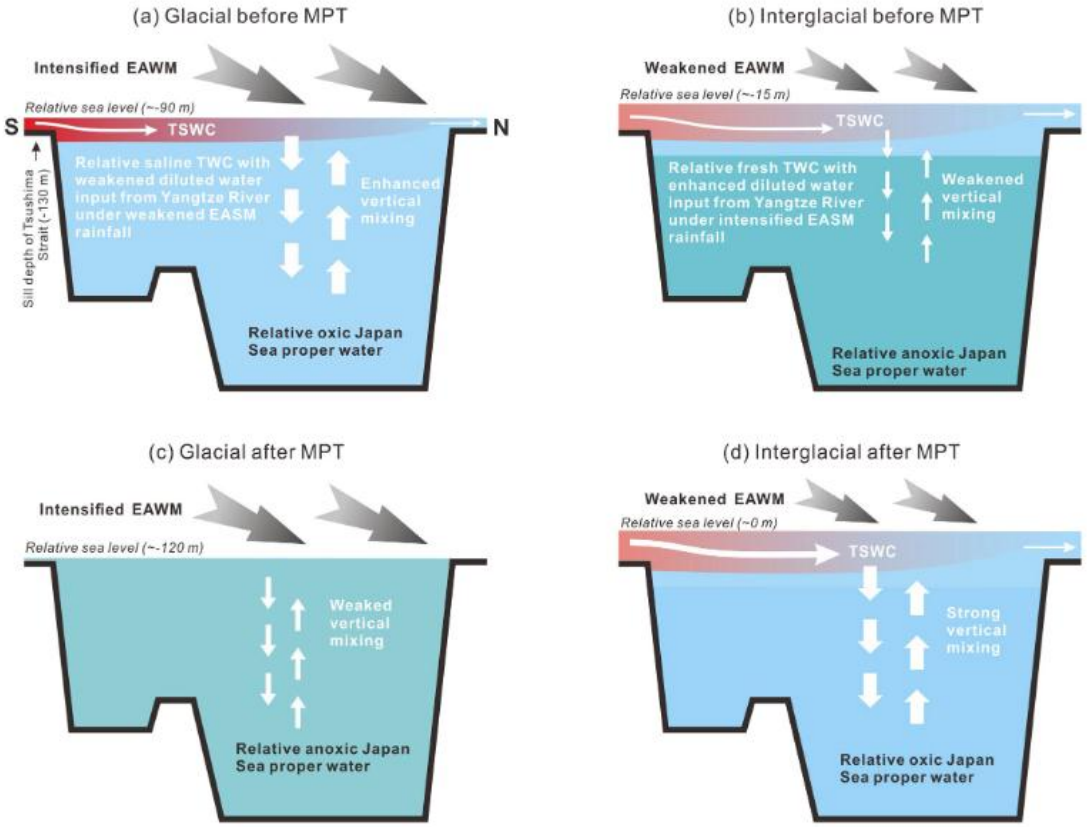

Figure 2. Schematic diagram of the Japan Sea redox evolution during glacial-interglacial cycles before (a–b) and after the MPT (c–d).

4. 中国西南地区干燥-湿润模式的不同位面

翻译人：杨会会 11849590@mail.sustech.edu.cn

Liao, M N, Li K, Ni J, ***Different facets of dryness/wetness pattern in southwestern China over the past 27,000 years [J].****Climate of the Past, 2021.*

https://doi.org/10.5194/cp-2021-55

摘要：当前全球气候变化背景下，频繁发生的干旱引起了社会的广泛关注。预计从古气候学的角度对其成因和表现进行可以获得更综合的理解。中国西南地区受到了严重的季节性干旱的威胁。我们目前对该地区千年尺度的干湿过程的理解主要基于印度夏季风的变化。然而，陆地上水的变化并不总是跟随季风降雨，也依赖于蒸发和蒸腾作用过程中损失的水。本文中，我们基于艺龙湖（Yilong）的粒度，地球化学和孢粉记录，重建了过去 27 ka 以来的降雨强度，湖泊水份平衡和土壤水压指数（SWSI），以讨论中国西南云南中部地区气象、水文和土壤系统的长期关系和干燥/潮湿模式的差异。我们的结果表明，降水、水文平衡和土壤湿度的长期变化轨迹之间不完全一致。在降雨量较低的时期，水文平衡和土壤湿度主要受控于温度导致的蒸发的变化。这导致了在末次冰盛期和新仙女木时期，降雨与水文平衡和土壤湿度之间相反的状态。在降雨量较高的时期 — 早晚全新世，湖泊表面较强的蒸发抵消了降水增加对水文平衡的影响。但同时，丰富的降雨和浓密的植被冠层避免了，可能由于温度增加引起的土壤水分亏缺。综上所述，滇中地区的水文平衡更易受到温度变化的影响，而在千年尺度上植被的变化可能进一步调节了土壤水分。因此，在未来气候变暖的背景下，滇中地区地表水紧缺可能会更严重。但对于土壤系统来说，重新造林的努力可能缓解该地区的土壤水分缺失。

ABSTRACT: Frequently happened meta-droughts have arisen broad social attention under current global climate change. A paleoclimatic perspective is expected to gain our understanding on the causes and manifestation more comprehensively. Southwestern China has been threatened by severe seasonal droughts. Our current knowledge of millennial-scale drying/wetting processes in this region is primarily based on the variability of the Indian Summer Monsoon. However, water availability over land does not always follow the monsoonal precipitation but also depends on water

loss from evaporation and transpiration. Here, we reconstructed precipitation intensity, lake hydrological balance and soil water stress index (SWSI) covering the last 27,000 yr, based on grain size, geochemical and pollen records from Yilong Lake, to discuss the long-term nexus and discrepancies of dryness/wetness patterns in meteorological, hydrological and soil systems in central Yunnan region, SW China. Our results show that the long-term change trajectories among precipitation, hydrological balance and soil moisture were not completely consistent. During periods of low precipitation, hydrological balance and soil moisture were primarily controlled by temperature-induced evaporation change. This caused opposite status of precipitation with hydrological balance and soil moisture during the Last Glacial Maximum and Younger Dryas. During periods of high precipitation — the early to late Holocene, intensified evaporation from the lake surface offset the effects of increased precipitation on hydrological balance. But meanwhile, abundant rainfall and dense vegetation canopy avoided soil moisture deficit that might result from rising temperature. To sum up, hydrological balance in central Yunnan region was more vulnerable to temperature change while soil moisture could be further regulated by vegetation changes on millennial scale. As such, under future climate warming, surface water shortage in central Yunnan region can be even more serious. But for soil systems, efforts to reforestation may bring some relief to soil moisture deficit in this region.

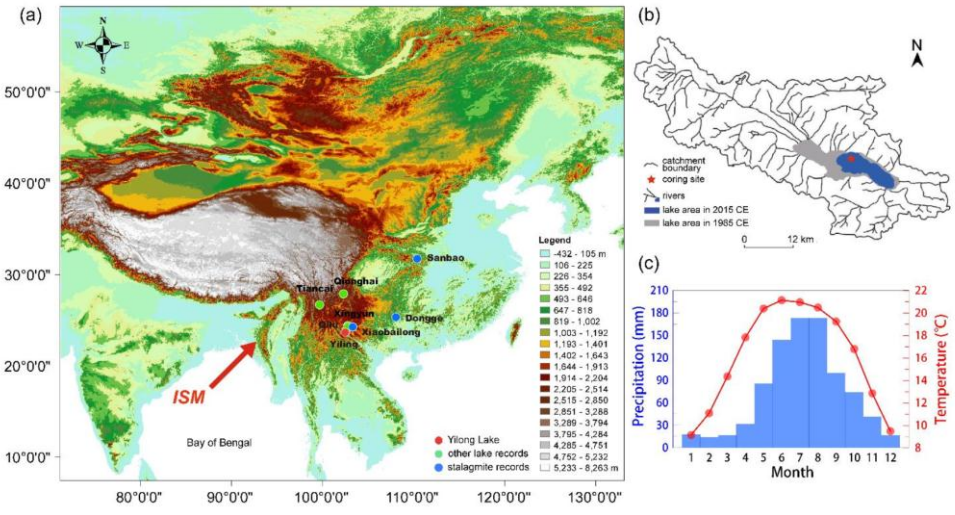

Figure 1. (a) Map showing the locations of Yilong Lake, other lake and stalagmite records; (b) catchment of the lake and the location of the core YLH; (c) average monthly temperature and precipitation during 1951–2017 CE (China Meteorological Data Service Centre, ttps://data.cma.cn/en)

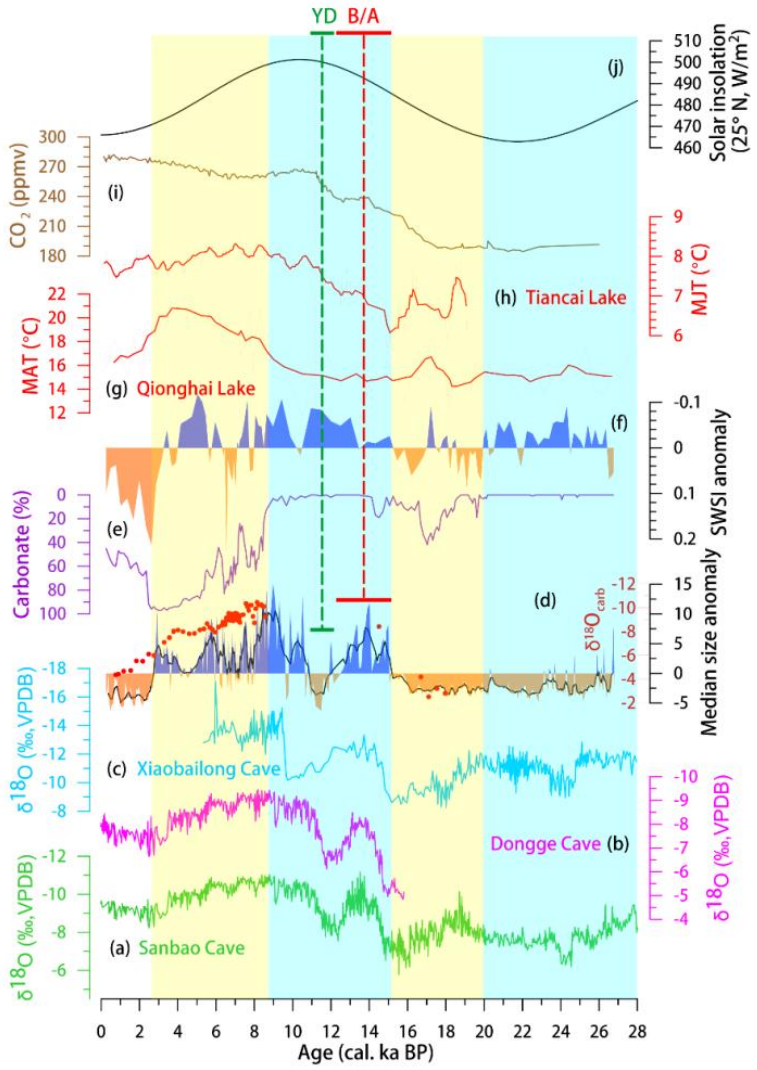

Figure 2. Stalagmite $\delta^{18}O$ records from Sanbao Cave (Cheng et al., 2016) (a), Dongge Cave (Dykoski et al., 2005) (b), and Xiaobailong Cave (Cai et al., 2015) (c); median size and $\delta^{18}O_{carb}$ (d), carbonate content (e), pollen-based reconstructed SWSI (f) from Yilong Lake (this study); (g) brGDGT-derived mean annual temperature (MAT) from Qionghai Lake (Wang et al., 2020); (h) chironomid-mean July temperature (MJT) from Tiancai Lake (Zhang et al., 2019a); (i) CO_2 concentration from Antarctic ice core record (Ahn et al., 2004); (j) Summer insolation curve for 25 ℃N.

5. 青藏高原东北部临夏盆地早中始新世水文气候变化的环境磁学记录

翻译人：曹伟 11930854@qq.com

Feng Z T, Zhang W L, Zhang T, et al. ***Early-Middle Eocene Hydroclimate Variations Recorded by Environmental Magnetism in the Linxia Basin, NE Tibetan Plateau*** *[J].* ***Paleoceanography and Paleoclimatology****, 2021, 36, e2021PA004338.*

https://doi.org/10.1029/2021PA004338

摘要：尽管中亚新近纪气候变化重建对于理解全球变冷、亚洲季风演化和新生代青藏高原逐步抬升具有重要意义，但是由于缺乏相应连续完整的陆相记录和精确的年龄限制，该地区古近纪的古环境演化仍不明确。最近，在青藏高原东北部的临夏盆地发现了一个新的河流沉积层序，其磁性地层年龄从 53 到 40 Ma，为了解亚洲内陆始新世气候变化提供了一个窗口。根据这一河流沉积序列，我们基于岩石磁学和漫反射光谱的组合方法，展示了早始新世-中始新世的水文气候变化。我们的研究结果表明，51.7 Ma 时河流沉积物的磁性增强是由于在相对潮湿的环境中，通过强烈侵蚀和运输，来自周围山脉的大量单畴磁铁矿输入所致。随后，在 47.6 Ma 时，漫滩沉积物的磁性减弱对应于在长期干燥环境中通过低温氧化产生的赤铁矿浓度增加。通过对比古气候指标，如邻近盆地的有机地球化学和岩石磁学，青藏高原东北部的构造变形，以及副特提斯洋的海平面变化表明，该地区始新世中早期由相对湿润气候到干燥气候的水气候变化主要受全球气候变化控制，并且可能与青藏高原的隆升叠加。

ABSTRACT: Although Neogene climate change reconstruction in central Asia is important for understanding global cooling, Asian monsoon evolution, and the Tibetan Plateau stepwise uplift during the Cenozoic, the paleoenvironmental evolution during the Paleogene in this region is still ambiguous due to a lack of corresponding continuous and complete terrestrial records with precise age constraints. Recently, a new fluvial sedimentary sequence with magnetostratigraphic ages spanning from ~53 to 40 Ma was found in the Linxia Basin, NE Tibetan Plateau, thereby providing a window to understand Eocene climate change in the Asian interior. From this fluvial sedimentary sequence, we present early-middle Eocene hydroclimate variations based on a combined method of

rock magnetism and diffuse reflectance spectroscopy. Our results show magnetic enhancement of fluvial sediments at 51.7 Ma resulted from abundant single-domain magnetite inputs from the surrounding mountains through strong erosion and transport in a relatively wet environment. Subsequently, at 47.6 Ma, magnetic weakening of floodplain sediments corresponds to an increase in hematite concentrations produced via low-temperature oxidation in a prolonged dry environment. Comparisons of paleoclimatic proxies, such as organic geochemistry and rock magnetism from neighboring basins, tectonic deformation of the NE Tibetan Plateau, and sea level change in the Paratethys Sea suggest that the hydroclimate variation from relatively wet to dry climate in the early-middle Eocene in this area was mainly controlled by global climatic change and probably superimposed by the uplift of the Tibetan Plateau.

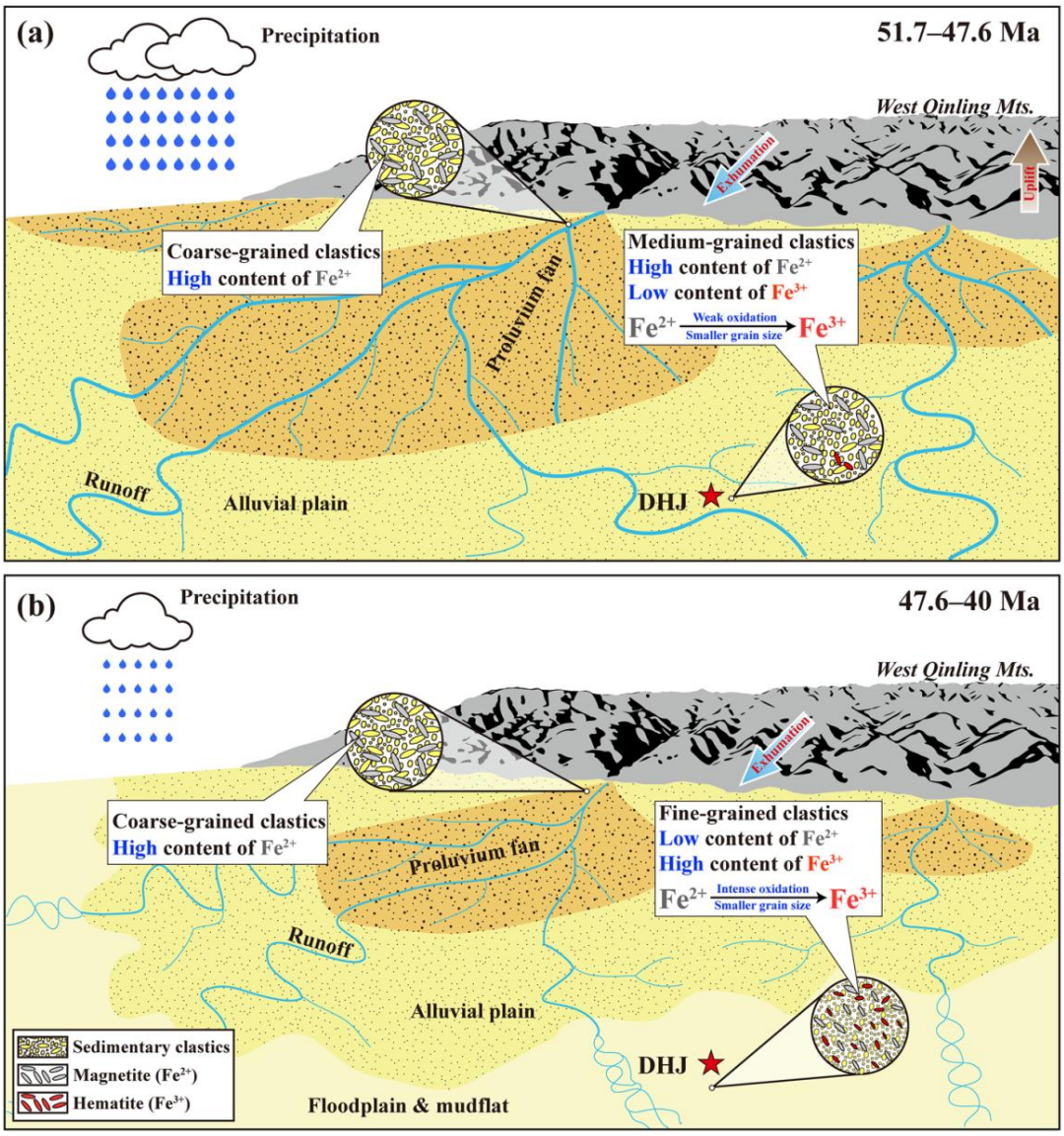

Figure 1. Depositional environment and variation in magnetic minerals in the Linxia Basin sediments during the early-middle Eocene. Note that the magnetic minerals in the sediments during 51.7-47.6 Ma are dominated by magnetite, which is transported from surrounding mountains (a). Subsequently, during 47.6-40 Ma, the sediments are rich in hematite, which transforms from magnetite via low-temperature oxidation in the environment with frequent episodes of prolonged dryness (b).

6. 对 8.2 ka 事件期间海平面上升幅度的新估计

翻译人：李海 12031330@mail.sustech.edu.cn

Obrist-Farner J, Brenner M, Stone J R, et al. ***New estimates of the magnitude of the sea-level jump during the 8.2 ka event*** *[J]. Geology, 2021.*

https://doi.org/10.1130/G49296.1

摘要：作者分析了危地马拉 Izabal 湖沿岸的沉积物岩芯，以推断该湖全新世期间生物地球化学的变化。在 8370 cal yr BP，海水进入该湖，目前距离加勒比海岸~38 km。高纬度的 Agassiz 湖和 Ojibway 湖的早全新世排水与 Izabal 湖的海洋洪水之间的时间相关性表明这两个过程之间存在因果关系。作者的数据表明海平面相对上升了 2.60 ±0.88 m，大于先前对 8.2 ka 事件期间海平面上升的估计。然而，推断的海平面上升不能仅用 Agassiz 湖和 Ojibway 湖排水过程中释放的水量来解释。相反，作者认为之前的研究低估了 Agassiz 湖和 Ojibway 湖的排放量，或者当时额外的融水来源导致了全球海平面上升。

ABSTRACT: We analyzed sediment cores from coastal Lake Izabal, Guatemala, to infer Holocene biogeochemical changes in the lake. At ca. 8370 calibrated yr B.P. (cal. yr B.P.), marine waters entered the lake, which presently lies ~38 km from the Caribbean coast. Temporal correlation between Early Holocene drainage of high-latitude Lakes Agassiz and Ojibway (in North America) and marine flooding of Lake Izabal suggests a causal link between the two processes. Our data indicate a relative sea-level jump of 2.60 ± 0.88 m, which is larger than previous estimates of sea-level rise during the 8.2 ka event. The inferred sea-level jump, however, cannot be explained solely by the volume of water released during drainage of Lakes Agassiz and Ojibway. Instead, we propose that previous studies underestimated the magnitude of Lakes Agassiz and Ojibway discharge, or that additional meltwater sources contributed to global sea-level rise at that time.

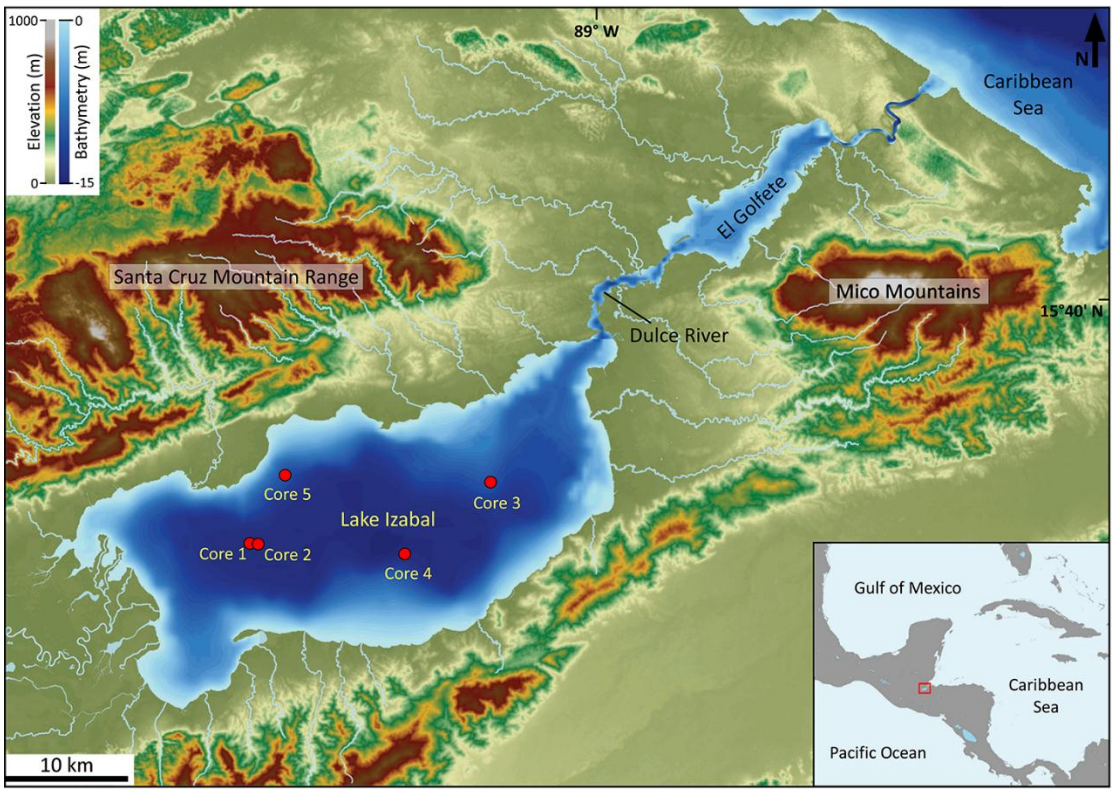

Figure 1. Bathymetric map of Lake Izabal (Guatemala) and topography of the area. Red circles indicate sites of sediment core collection. Inset map shows Central America and surrounding regions; the location of Lake Izabal in eastern Guatemala is indicated by the red box.

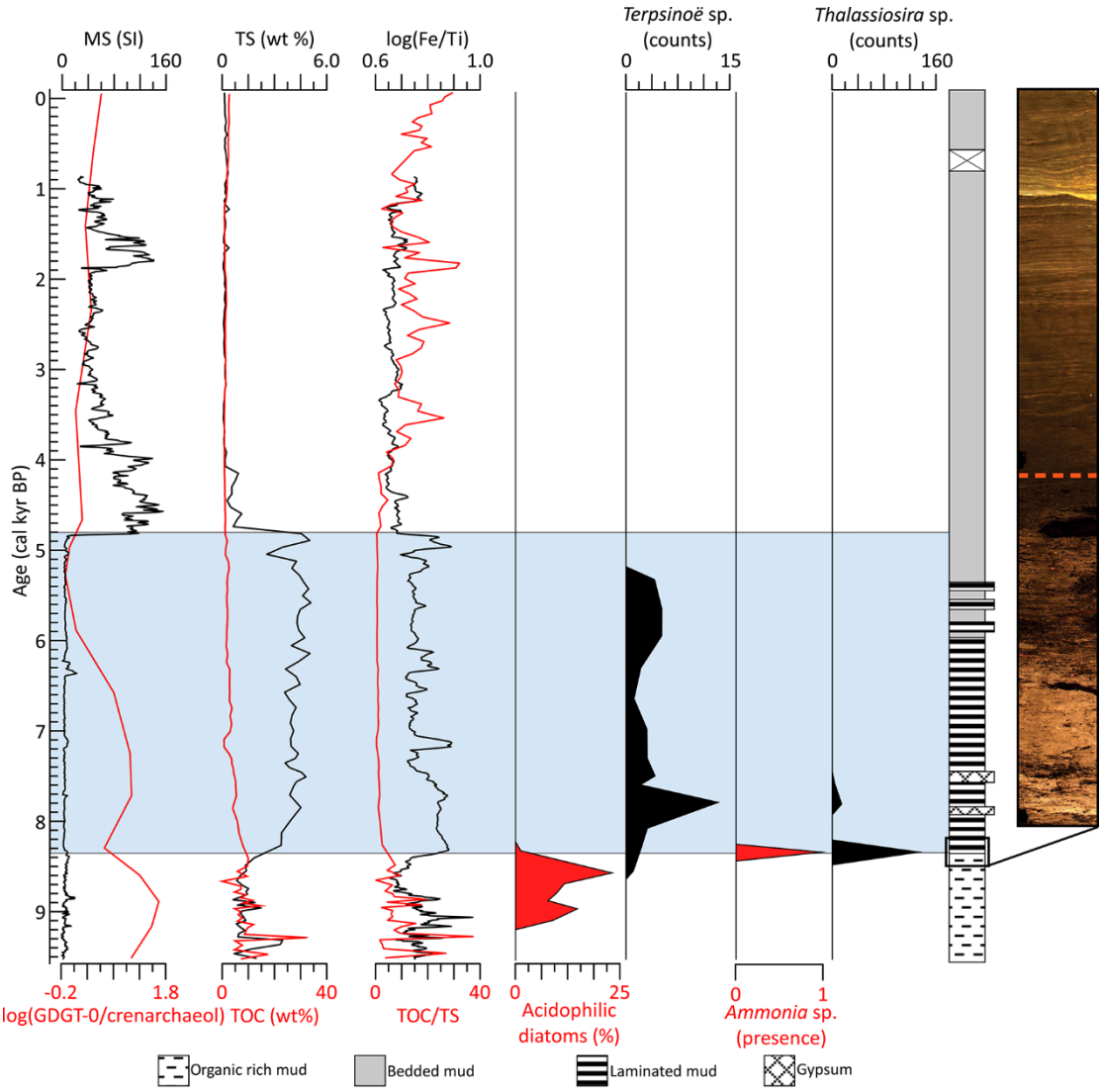

Figure 2. Sediment characteristics versus age in calibrated yr B.P. (cal. yr B.P.) for Core 5, with a simplified lithological column to the right. The blue zone highlights the interval when Lake Izabal (Guatemala) changes to a saline and anoxic lake. The first (left) panel shows stratigraphic variations in magnetic susceptibility (MS) and the log(GDGT-0/crenarchaeol) ratio; both are proxies for anoxic conditions. The second panel shows total organic carbon (TOC) and total sulfur (TS) content in the sediment. The sudden increase in TS at ca. 8370 cal. yr B.P. occurs immediately above the flooding surface. The third panel shows the log(Fe/Ti) and TOC/TS ratios. Low values of the TOC/TS ratio, a proxy to differentiate marine from freshwater deposits, coincide with an increase in the log(Fe/Ti), a proxy for anoxic conditions. Before ca. 8370 cal. yr B.P., Lake Izabal was characterized by acidophilic diatoms (red curve in fourth panel). The mesohaline diatom Terpsino ë sp. (black curve in fifth panel) appears immediately before the flooding surface and the foraminiferan Ammonia sp. (red curve in sixth panel), and the diatom Thalassiosira sp. (black curve in seventh panel) appear at

ca. 8370 cal. yr B.P. Photo on the right shows the transition from organic-rich mud to sub-millimeter laminated mud after the flooding surface (red dashed line). Photo shows 40 cm of Core 5.

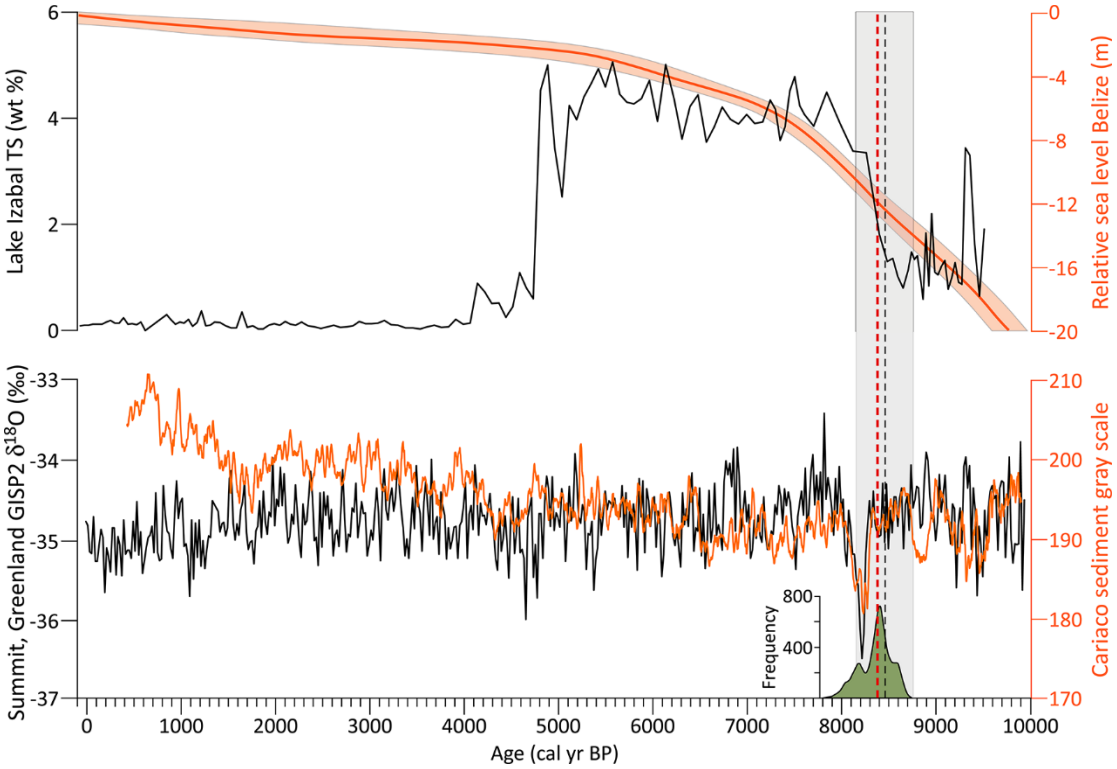

Figure 3. Records of sea-level rise in the Caribbean region and during the 8.2 ka event. Bottom plot shows a decrease in the Cariaco Basin sediment gray scale (red line) that resulted from windier conditions caused by high-latitude cooling (Hughen et al., 1996) and a decrease in oxygen isotope values in Greenland (black line), which reflect lower temperatures (Stuiver et al., 1995). Upper plot shows the increase in total sulfur (TS; black line) after the flooding event in Lake Izabal (Guatemala) and the sea-level curve (red line) and 1σ uncertainty (light red envelope) from Belize (Khan et al., 2017). Vertical black dashed line and gray box show the age and 1σ uncertainty for the drainage of Lakes Agassiz (in central North America) and Ojibway (in Canada) (Barber et al., 1999). Vertical red dashed line shows the mean age, and the green histogram at the bottom shows the frequency of age estimates of the flooding event in Lake Izabal.

7. 来自阿拉斯加湾 IODP 341 航次 U1418 和 U1419 站点高分辨率倾角记录

翻译人：张琪 zhangq7@sustech.edu.cn

Velle J H, Walczak M H, Reilly B, et al., ***High resolution inclination records from the Gulf of Alaska, IODP Expedition 341 Sites U1418 and U1419*** *[J]. Geophysical Journal International, 2021, 229, 1, 345-358.*

https://doi.org/10.1093/gji/ggab479

摘要：国际大洋钻探计划(IODP) 341 航次在南阿拉斯加大陆坡上恢复了一段包含过去 43000 年倾角信息的沉积物样品，样品分辨率与定年良好。U1419 站点具有世界上最高分辨率年代学记录（来自 173 个放射性碳定年的约束），可以用来研究百年至千年尺度上的古地磁长期变化（PSV）。该记录还具有一段晚更新世沉积记录，沉积速率大约 100 cm/千年， 同时在顶部保留了一段分辨率较低的全新世 PSV 记录。作者利用逐步 AF 退磁方法研究了 112 m 长 U1419U 形拼接沉积物记录中的天然剩磁与实验室诱导剩磁。测量了 95 个样品的磁滞回线，9 个样品的 IRM 获得曲线，用以分析样品的磁畴状态、矫顽力与矿物学鉴定。由于样品岩性、磁性、沉积与沉积后的过程方面的复杂性，U1419 站点沉积物不适合进行古强度的研究，且不能进行较好的倾角的重建。含钛磁铁矿随深度增加溶解导致 NRM 强度和信号降低，在更高场的退磁步骤中更加明显。因此，在 20 mT AF 退磁步骤后测得的倾角可提供可靠的方向记录。当去除几个受沉积或取样变形影响的层段之后，倾角问题可以得到很好的解决。来自附近 U1418 站点的 19 个放射性碳测年的新年代学模型，验证了在 U1419 站点观测到的百年至千年尺度上的变化。与其它来自东太平洋和北美西部的独立定年记录比较，这些站点可能能够记录区域地磁的变化。因此，这一新的高分辨率和年代良好的倾角记录，特别是在 15-30 cal kye BP 之间，提供了新的地磁场信息和区域对比工具，可以用来探索这一未被普遍研究过的地区。

ABSTRACT: International Ocean Drilling Program (IODP) Expedition 341 recovered sediments from the south Alaska continental slope that preserves a well resolved and dated inclination record

over most of the past ~43 000 yr. The Site U1419 chronology is among the highest resolution in the world, constrained by 173 radiocarbon dates, providing the ability to study Palaeomagnetic Secular Variation (PSV) on centennial to millennial timescales. This record has an exceptionally expanded late Pleistocene sedimentary record with sedimentation rates commonly exceeding 100 cm kyr–1, while also preserving a lower resolution Holocene PSV record at the top. Natural and laboratory-induced magnetic remanences of U1419 u-channels from the 112-m-long spliced record were studied using stepwise AF demagnetization. Hysteresis loops were obtained on 95 and IRM acquisition curves on 9 discrete samples to facilitate magnetic domain state, coercivity and magnetic mineralogical determinations. Due to complexities related to lithology, magnetic mineralogy, and depositional and post-depositional processes, Site U1419 sediments are not suitable for palaeointensity studies and declination could not be robustly reconstructed. Progressive (titano-)magnetite dissolution with depth results in decreasing NRM intensity and signal-to-noise that is exacerbated at higher demagnetization steps. As a result, inclination measured after the 20 mT AF demagnetization step provides the most reliable directional record. Inclination appears to be well resolved with removal of just a few intervals influenced by depositional and/or sampling and coring deformation. The shipboard inclination stack from nearby IODP Site U1418, on a new age model developed from 19 radiocarbon dates on U1418 and 18 magnetic susceptibility-based tie-points to site survey core EW0408-87JC, verifies centennial to millennial scale variations in inclination observed in U1419. Comparisons with other independently dated records from the NE Pacific and western North America suggest that these sites likely capture regional geomagnetic variability. As such, this new high-resolution and well-dated inclination record, especially robust between 15 and 30 cal kyr BP, offers new geomagnetic insights and a regional correlation tool to explore this generally understudied part of the world.

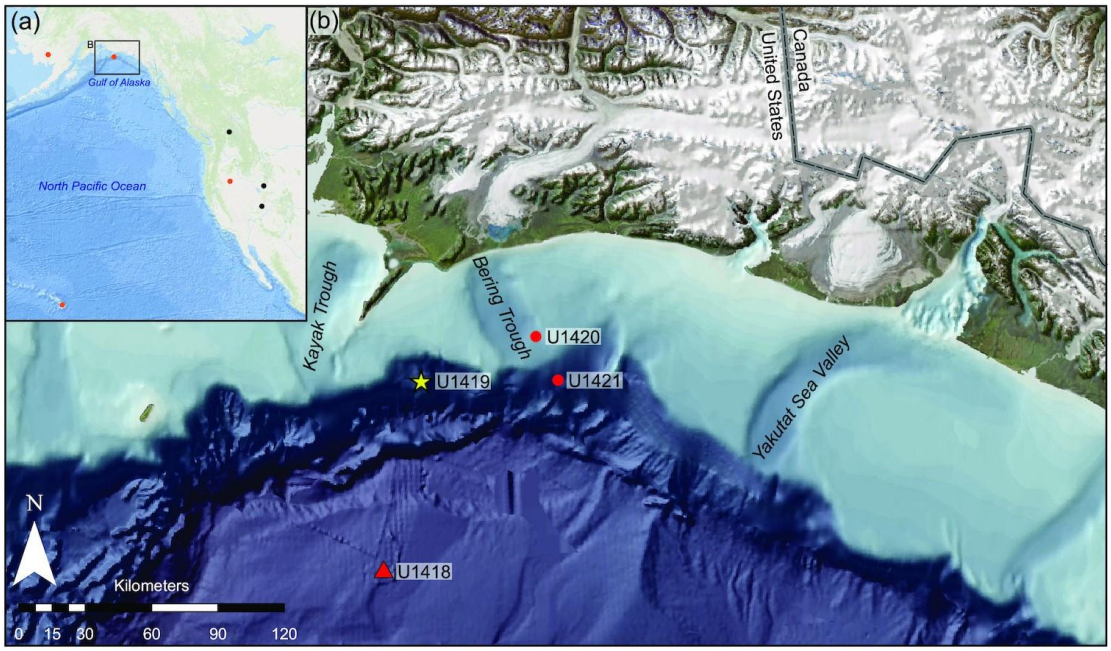

Figure 1. (a) Overview of the northeast Pacific region with locations of cores and sites incorporated in the NEPSIAS (Walczak et al. 2017) and WNAM17 (Reilly et al. 2018) stacks indicated in orange and black circles, respectively. (b) The Gulf of Alaska with IODP Expedition 341 drill Sites. Site U1419 is indicated by a yellow star which also marks the location of U1419 of site survey core EW0408-85JC mentioned in the text. The Surveyor Fan Site U1418 is indicated by a red triangle. This triangle also marks the location of core EW0408-87JC mentioned in the text.

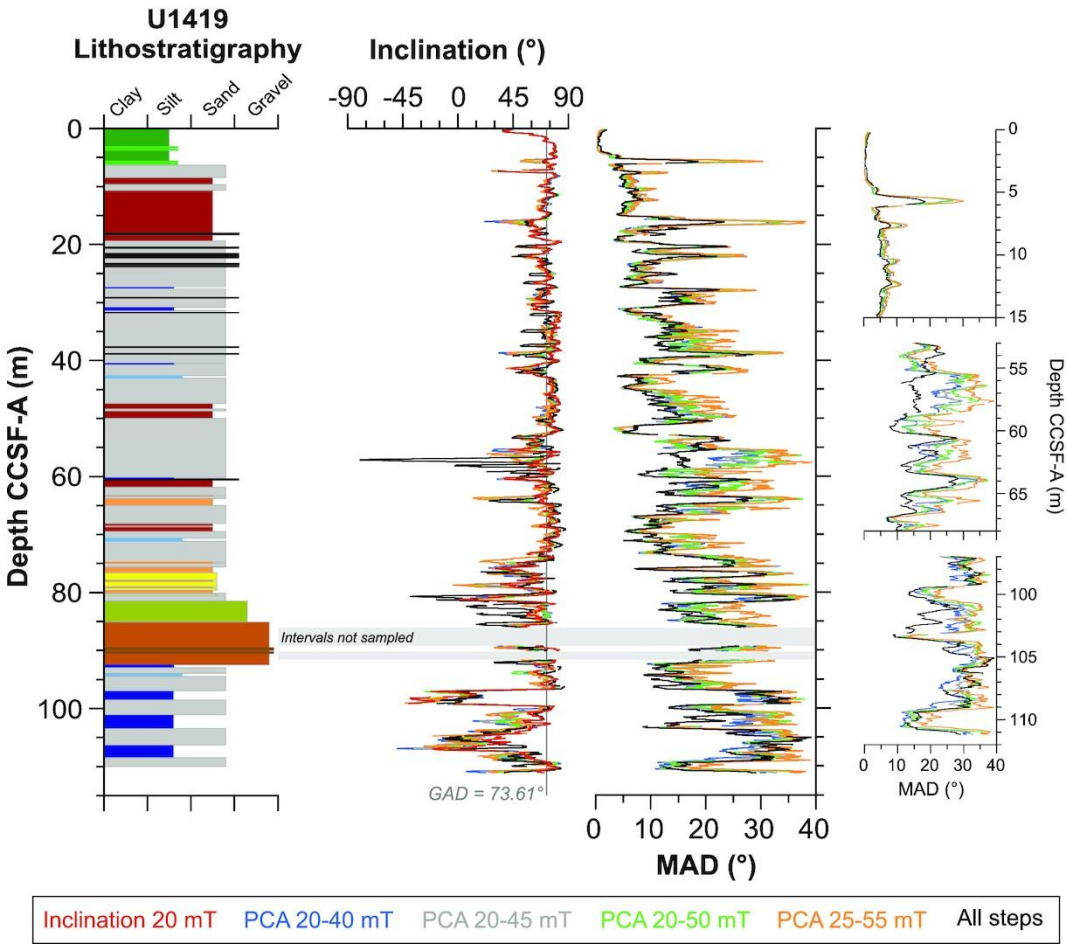

Figure 2. U1419 lithostratigraphy (modified from Penkrot et al. 2018), selection of PCA ranges for U1419 inclination and their associated MAD values, all with a 40-point smoothing. The inclination as measured at 20 mT is highlighted in red as it is described in more detail in the text. Selected intervals display examples of agreeing and diverging MAD values (right).

8. 内太阳系发电机

翻译人：张伟杰 12031188@mail.sustech.edu.cn

Tikoo S M, Evans A J. ***Dynamos in the Inner Solar System*** *[J]. Annual Review of Earth and Planetary Sciences, 2022, 50.*

https://doi.org/10.1146/annurev-earth-032320-102418

摘要：磁场发电机主要由行星核内导电液态金属的热化学对流产生。对流可以通过长期冷却来维持，并且可能通过核凝固相关的成分浮力来加强。此外，通过大型撞击、潮汐、轨道进动引起的核内流体的机械运动和外部扰动也有助于维持发电机磁场。当核-幔热流变为次绝热状态或特定的结晶状态抑制地核流体流动时，对流发电机停止。因此，探索整个太阳系磁场的历史对了解行星内部的热演化和化学演化提供了一个窗口。古地磁学和星体壳的剩磁研究阐明了岩质行星体的磁演化史。发电机古磁场记录已从 4 颗类地行星中的 3 颗、月球和几个小行星获得。发电机场的几何形貌、强度和寿命可以提供核和行星热演化的信息。本文，我们总结了最近基于航天器的地壳剩磁、岩石样品的古地磁和行星内部模型研究，揭示了水星、地球、火星、月球和几个星子的磁性和演化历史，并讨论了未来的探索和发现的途径。

ABSTRACT: Dynamo magnetic fields are primarily generated by thermochemical convection of electrically conductive liquid metal within planetary cores. Convection can be sustained by secular cooling and may be bolstered by compositional buoyancy associated with core solidification. Additionally, mechanical stirring of core fluids and external perturbations by large impact events, tidal effects, and orbital precession can also contribute to sustaining dynamo fields. Convective dynamos cease when the core-mantle heat flux becomes subadiabatic or if specific crystallization regimes inhibit core fluid flows. Therefore, exploring the histories of magnetic fields across the Solar System provides a window into the thermal and chemical evolution of planetary interiors. Here we review how recent spacecraft-based studies of remanent crustal magnetism, paleomagnetic studies of rock samples, and planetary interior models have revealed the magnetic and evolutionary histories of Mercury, Earth, Mars, the Moon, and several planetesimals, as well as discuss avenues for future exploration and discovery. Paleomagnetism and remanent crustal magnetism studies elucidate the magnetic histories of rocky planetary bodies. Records of ancient dynamo fields have

been obtained from 3 out of 4 terrestrial planets, the Moon, and several planetesimals. The geometries, intensities, and longevities of dynamo fields can provide information on core processes and planetary thermal evolution.

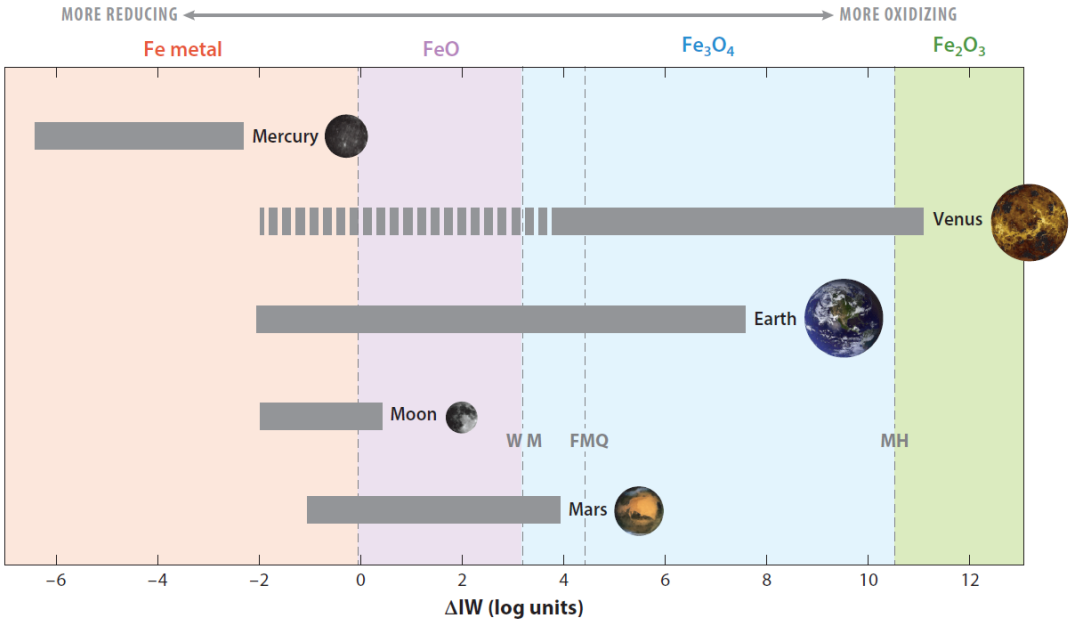

Figure 1. Oxygen fugacity ranges for inner Solar System bodies relative to the iron-wüstite (IW) buffer and examples of resulting magnetic mineralogies. For example, more reducing environments will preferentially form Fe metal whereas more oxidizing conditions will produce increasingly oxidized phases such as magnetite and hematite. The relative positions of the wüstite-magnetite (WM), fayalite-magnetite-quartz (FMQ), and magnetite-hematite (MH) buffers at ~1,200 ℃ are shown with vertical dashed lines for reference. Oxygen fugacities are sourced from Fegley et al. (1995), Kelley & Cottrell (2009), Strauss et al. (2016), and references therein. Figure adapted from Strauss et al. (2016), figure 1.

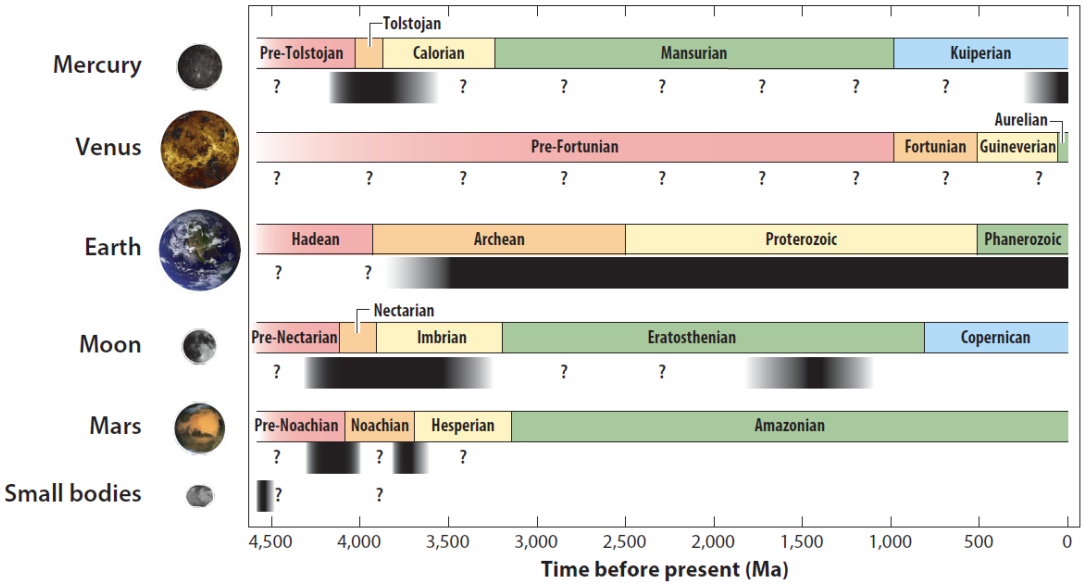

Figure 2. Timing of inner Solar System dynamos as inferred from remanent crustal magnetism, paleomagnetism, and spacecraft detection of active dynamo fields. Black bars and shaded intervals denote time periods interpreted to correspond with dynamo activity, whereas question marks denote time periods where data are lacking to infer the presence or absence of a dynamo. Figure adapted with permission from Lapôtre et al. (2020), figure 1.

9. 热带季节性变化控制着海洋浮游植物的周期性演化

翻译人：仲义 zhongy@sustech.edu.cn

Luc Beaufort, Clara T. Bolton, Anta-Clarisse Sarr., et al, ***Cyclic evolution of phytoplankton forced by changes in tropical seasonality*** *[J] Nature, 2021.*

https://doi.org/10.1038/s41586-021-04195-7.

摘要：尽管地球轨道变化的作用是驱动全球气候周期性变化得到公认，但是其演化方面的重要作用仍然未知。颗石藻作为化石遗迹，是一个关键性钙化浮游植物群落，可以用来详细评估轨道尺度气候变化对进化的影响，它们在海洋沉积物中的丰富程度以及它们形态的保存来适应变化的环境。进化遗传分析通过更新世化石颗石藻形态学方法来反演物种辐射事件。本文中，作者基于高分辨率的颗石藻结果，展示了过去 2.8 百万年以来颗石藻形态演化历史，该形态主要由地球轨道的自转周期约为 10 万年和 40 万年周期所控制。结合地球系统模型和海洋生物地球化学模型显示了季节性周期偏心率调节，会直接影响热带海洋生态循环的多样性。海洋表面季节性的减弱有利于中等大小的颗石藻生活，促进了颗石藻碳酸盐的输出和保存；而增强的季节性有利于更大范围的颗石藻大小和减少碳酸盐输出。作者推测浮游植物演化的偏心率变化反映了全球碳循环记录过程中的强烈的 405 千年周期性变化。

ABSTRACT: Although the role of Earth's orbital variations in driving global climate cycles has long been recognized, their effect on evolution is hitherto unknown. The fossil remains of coccolithophores, a key calcifying phytoplankton group, enable a detailed assessment of the effect of cyclic orbital-scale climate changes on evolution because of their abundance in marine sediments and the preservation of their morphological adaptation to the changing environment. Evolutionary genetic analyses have linked broad changes in Pleistocene fossil coccolith morphology to species radiation events. Here, using high-resolution coccolith data, we show that during the last 2.8 million years the morphological evolution of coccolithophores was forced by Earth's orbital eccentricity with rhythms of around 100,000 years and 405,000 years—a distinct spectral signature to that of coeval global climate cycles. Simulations with an Earth System Model coupled with an ocean

biogeochemical model show a strong eccentricity modulation of the seasonal cycle, which we suggest directly affects the diversity of ecological niches that occur over the annual cycle in the tropical ocean. Reduced seasonality in surface ocean conditions favours species with mid-size coccoliths, increasing coccolith carbonate export and burial; whereas enhanced seasonality favours a larger range of coccolith sizes and reduced carbonate export. We posit that eccentricity pacing of phytoplankton evolution contributed to the strong 405,000-year cyclicity that is seen in global carbon cycle records.

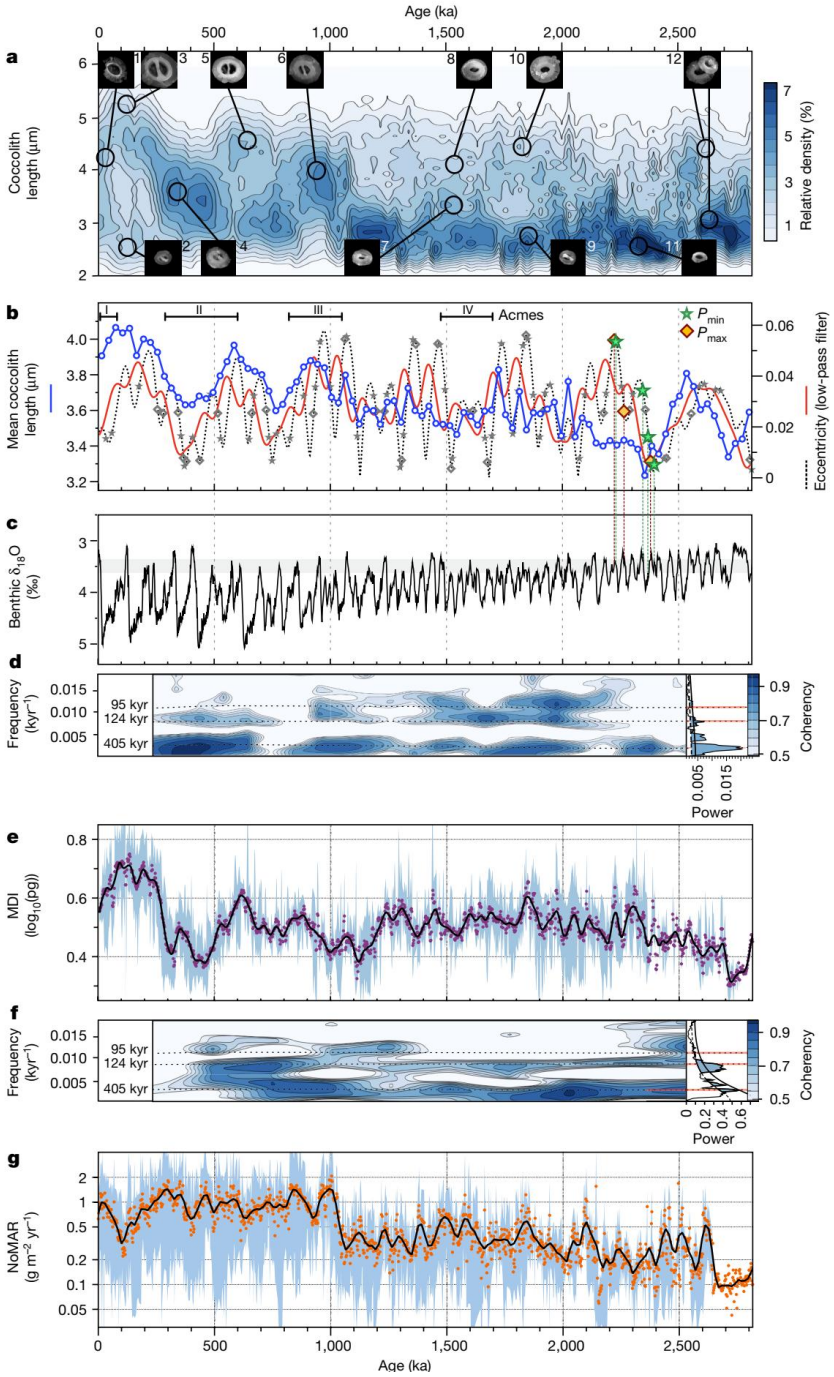

Figure 1. Noelaerhabdaceae coccolith morphology and accumulation, eccentricity, and climate over the last 2.8 million years. a, Frequency contour plot of multi-site stacked coccolith length (Methods). Scanning electron microscope images represent examples of the diversity of Noelaerhabdaceae morphologies over time. 1,Emiliania huxleyi; 2,Gephyrocapsa ericsonii; 3,Gephyrocapsa oceanica; 4, Gephyrocapsa caribbeanica; 5–6,Gephyrocapsa omega; 7–8, mid-sizeGephyrocapsa; 9, small Gephyrocapsa; 10, Pseudemiliania ovata; 11, Reticulofenestra minuta; 12, left: P. ovata, right: R. minutula. b, Mean coccolith length in the stack (blue), plotted with Earth's eccentricity23 (dotted black line) and low-pass-filtered eccentricity with an angular frequency of 0.021 kyr−1 (red). Described Noelaerhabdaceae acmes19–21 are shown as black bars (I,E. huxleyi; II,G. caribbeanica; III and IV, mid-sizeGephyrocapsa). Coloured stars and diamonds on the eccentricity curve show the timing of actual orbital configurations used in model simulations (Pmax, precession with perihelion in December; Pmin, precession with perihelion in June); smaller grey symbols indicate times throughout the record with similar eccentricity and precession configurations to those modelled (Methods).c, LR04 benthic foraminiferal δ18O stack22. Grey band illustrates the small range of benthic δ18O between model simulations. d, Left, evolutive cross-spectral analysis between MDI and eccentricity (Methods). Colour-scale shows coherency (90% confidence level (CL) above 0.7); horizontal dashed lines show eccentricity periods. Right, MTM spectral analysis of detrended MDI stack. Shaded areas are above the CL90% (dashed line). Solid black line is CL95%. e, MDI stack (2-kyr resolution) (Methods). f, Left, evolutive cross-spectral analysis between NoMAR and MDI. CLs as in d(left). Right, MTM spectral analysis of detrended NoMAR stack. CLs as in d(right). g, NoMAR stack (2-kyr resolution; see Methods). MDI and NoMAR stacks are smoothed with a Loess function, and blue shading shows maximum and minimum values across all records.

10. 跨越上新世-更新世过渡时期的东赤道太平洋的稳定生物生产力

翻译人：王敦繁 Dunfan-w@foxmail.com

Jakob, K. A., Ho, S. L., Meckler, A. N., Pross, J., Fiebig, J., Keppler, F., & Friedrich, O. ***Stable biological production in the eastern equatorial Pacific across the Plio- Pleistocene transition (~3.35–2.0 Ma) [J]****. Paleoceanography and Paleoclimatology, 2021, 36, e2020PA003965.*

https://doi. org/10.1029/2020PA003965

摘要：东赤道太平洋(EEP)内的上升流是地球气候的一个关键因素，因为它支持目前 10%的生物生产力。正确理解上新世-更新世过渡时期 EEP 上升流的动力特征，对理解人类世大气二氧化碳上升导致的近期气候变暖事件意义重大。前人已经对东太平洋以东地区进行了深入研究，然而赤道上升流的变化却很少受到注意。因此，我们对来自大洋钻探计划 849 站点新的指标记录进行了研究，该站点位于 EEP 上升流区，目标区间(~ 3.35-2.0 Ma)包括了从北半球冰川作用(iNHG)增强为特征的上新世-更新世过渡时期。我们利用底栖生物 $\delta^{18}O$ 重建了该孔高分辨率年龄模型，并利用堆积速率和底栖生物 $\delta^{13}C$ 评估了生产力净输出量。我们的记录表明在整个 iNHG 的长期时间尺度上生产力净输出是稳定的。我们认为，以下过程控制了该站位的初级生产力的长期演化。首先，营养物质从高纬度地区输出到 EEP 区；然后，该时期太平洋营养线逐次浅滩化；最后，含铁风尘的输入减少。

ABSTRACT: Upwelling within the Eastern Equatorial Pacific (EEP) Ocean is a key factor for the Earth's climate because it supports >10% of the present-day biological production. The dynamics of upwelling in the EEP across the Plio-Pleistocene transition—an interval particularly relevant for understanding near-future warming due to Anthropocene-like atmospheric carbon-dioxide levels—have been intensively studied for the region east of the East Pacific Rise. In contrast, changes of the equatorial upwelling regime in the open Pacific Ocean west of this oceanographic barrier have received markedly less attention. We therefore provide new proxy records from Ocean Drilling Program Site 849 located within the EEP open-ocean upwelling regime. Our target interval (~3.35–2.0 Ma) covers the Plio-Pleistocene transition characterized by the intensification of Northern

Hemisphere Glaciation (iNHG). We use benthic δ18O values to generate a new, high-resolution age model for Site 849, and sand-accumulation rates together with benthic δ13C values to evaluate net export production. Although showing temporary substantial glacial-interglacial variations, our records indicate stability in net export production on secular timescales across the iNHG. We suggest the following processes to have controlled the long-term evolution of primary productivity at Site 849. First, nutrient export from the high latitudes to the EEP; second, a successive shoaling of the Pacific nutricline during the studied interval; and third, a simultaneous reduction in dust-borne iron input.

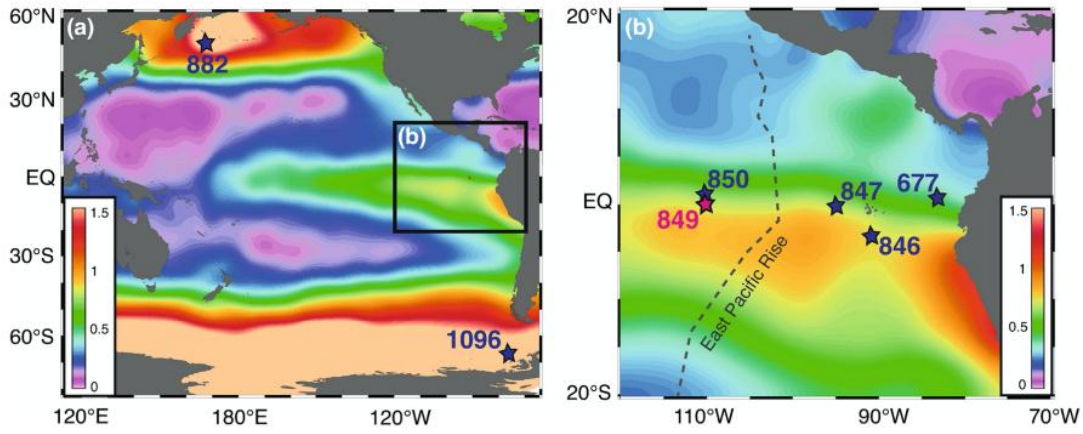

Figure 1. Locations of ODP Site 849 (red; this study) and other sites mentioned in the text (dark blue; previously published data sets) against a background map of modern annual sea-surface phosphate concentrations (in μmol l^{-1}) after World Ocean Atlas 2013 for (a), the Pacific and Southern Oceans and (b) the East Pacific Ocean. Regions with high sea-surface phosphate concentrations (and thus high nutrient availability) are typically associated with high rates of biological production.

11. 太平洋深部黑碳溶解过程

翻译人：王浩森 11930841@mail.sustech.edu.cn

Yamashita Y, Nakane M, Mori Y, et al. ***Fate of dissolved black carbon in the deep Pacific Ocean [J]. Nature communications****, 2022, 13(1): 1-7.*

https://doi.org/10.1038/s41467-022-27954-0

摘要：黑碳（BC）是生物和化石燃料燃烧的副产品，由于它可以在地球表面储存几个世纪到数千年，因此可能会影响气候。溶解的 BC（DBC）普遍存在于海洋中。然而，海洋中的 DBC 循环模式并没有得到很好的证明。本文展示了太平洋中 DBC 的盆地尺度分布，发现深太平洋中 DBC 的浓度沿着深海经向环流降低，且 DBC 浓度与表层氧利用率呈负相关，表层氧利用率指示太平洋深海下沉颗粒物的综合通量，这意味着 DBC 通过吸附在下沉颗粒物上而从深海转移到深海沉积物中。BC 在深海沉积物的埋藏通量估计为 0.040–0.085 PgC-yr^{-1}，相当于海洋吸收人造二氧化碳吸收量的 1.5–3.3%。

ABSTRACT: Black carbon (BC), a byproduct of biomass and fossil fuel combustion, may impact the climate because it can be stored on Earth's surface for centuries to millennia. Dissolved BC (DBC) occurs ubiquitously in the ocean. However, the DBC cycle in the ocean has not been well constrained. Here, we show the basin-scale distribution of DBC in the Pacific Ocean and find that the DBC concentrations in the deep Pacific Ocean decrease along with deep-ocean meridional circulation. The DBC concentration is negatively correlated with apparent oxygen utilization, a proxy of the integrated flux of sinking particles, in the deep Pacific Ocean, implying that DBC is removed from the deep ocean to abyssal sediments through sorption onto sinking particles. The burial flux of BC to abyssal sediments is estimated to be 0.040–0.085 PgC yr^{-1}, corresponding to 1.5–3.3% of the anthropogenic CO_2 uptake by the ocean.

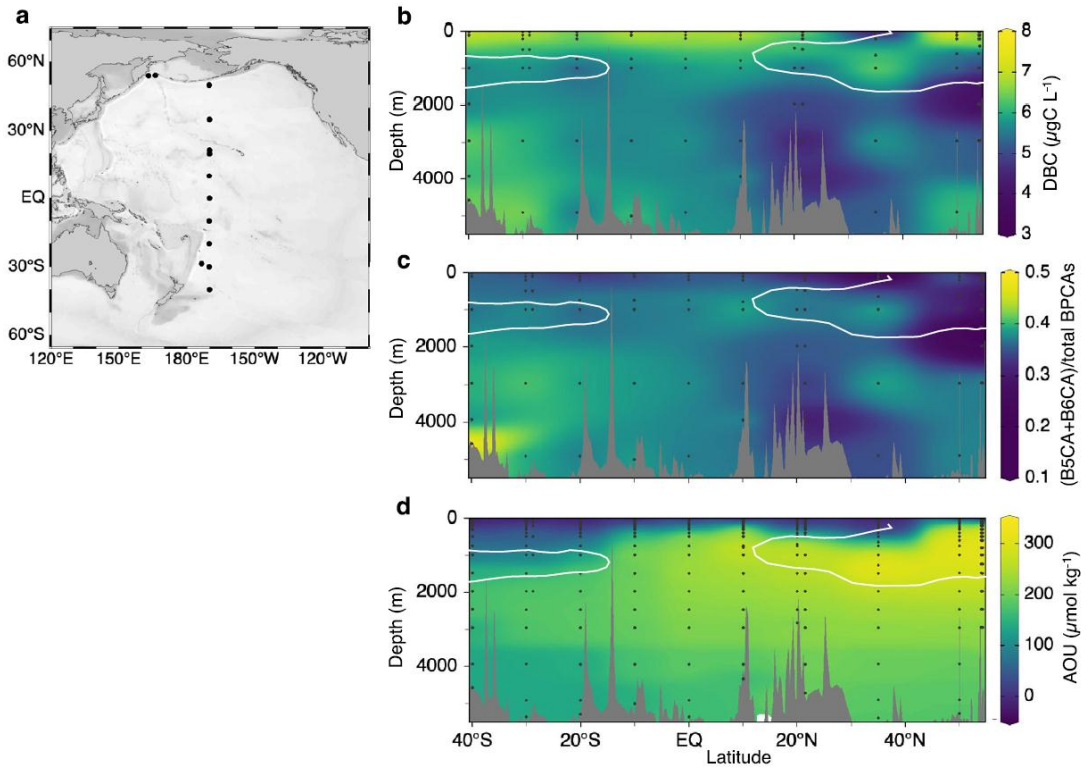

Figure 1. Meridional basin-scale distributions of dissolved black carbon (DBC) and apparent oxygen utilisation (AOU) in the Pacific Ocean. (a) Station locations. (b) DBC concentration (μgC L^{-1}). (c) The ratio of benzenepentacarboxylic acid (B5CA) + benzenehexacarboxylic acid (B6CA) to total benzenepolycarboxylic acids (BPCAs), which is an index of the condensation degree of DBC. (d) AOU (μmol kg^{-1}). The white solid lines in (b), (c) and (d) represent the subsurface salinity minima (salinity = 34.5).

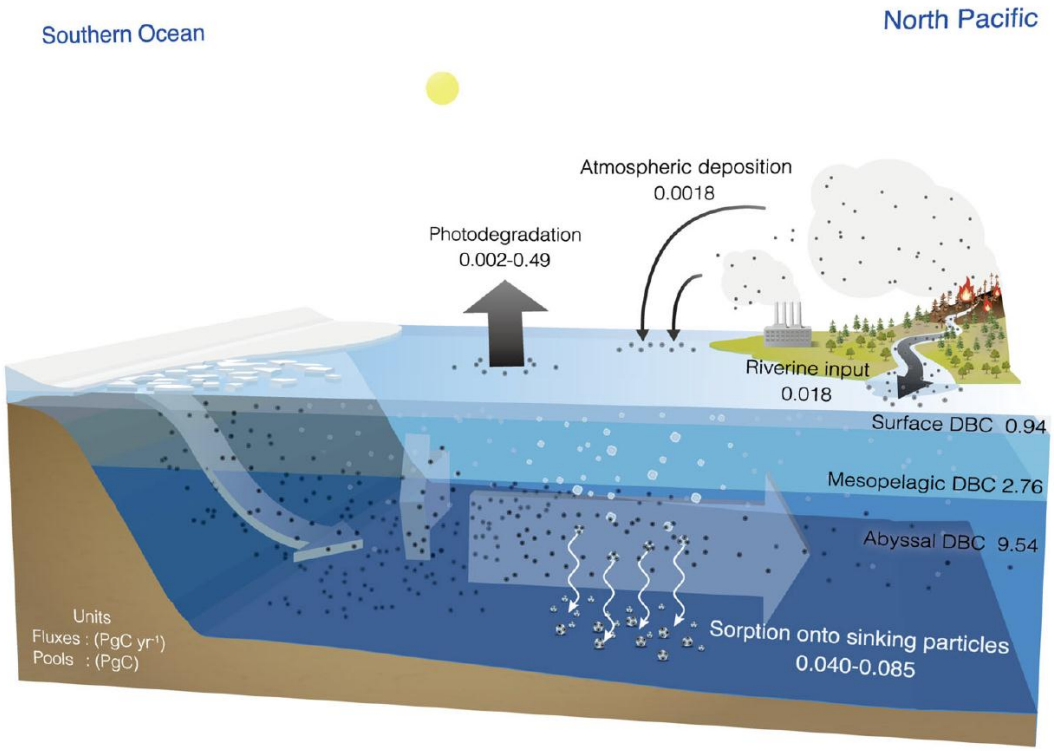

Figure 2. Schematics of the dissolved black carbon (DBC) cycle in the ocean, with emphasis on the Pacific Ocean. The pool sizes of surface DBC, mesopelagic DBC and abyssal DBC were estimated from the dissolved organic carbon (DOC) pool size and the DBC contribution to DOC. The riverine input flux was obtained from Jones et al. The atmospheric deposition flux is the dry deposition flux of water-soluble black carbon (BC) in aerosols. The photodegradation flux was obtained from Stubbins et al. The flux of sorption onto sinking particles was estimated in this study. The units of the pool sizes and fluxes are PgC and PgC $year^{-1}$, respectively.